Chemistry–A European Journal
Research Article
doi.org/10.1002/chem.202200004
Chemistry Europe
European Chemical Societies Publishing
www.chemeurj.org

Polycations Stabilised by Borosulfates: $[Au_3Cl_4][B(S_2O_7)_2]$ and the One-Dimensional Metal $[Au_2Cl_4][B(S_2O_7)_2](SO_3)$

Stefan Sutorius,[a] David van Gerven,[a] Selina Olthof,[b] Bertold Rasche,*[a] and Jörn Bruns*[a]

Abstract: (SO_4)-rich silicate analogue borosulfates are able to stabilise cationic cluster-like and chain-like aggregates. Single crystals of $[Au_3Cl_4][B(S_2O_7)_2]$ and $[Au_2Cl_4][B(S_2O_7)_2](SO_3)$ were obtained by solvothermal reaction with SO_3, and the electronic properties were investigated by means of density functional theory–based calculations. $[Au_3Cl_4][B(S_2O_7)_2]$ exhibits a cluster-like cation, and the cationic gold-chloride strands in $[Au_2Cl_4][B(S_2O_7)_2](SO_3)$ are found to resemble one-dimensional metallic wires. This is confirmed by polarisation microscopy.

Introduction

In recent years, interest in borosulfates has been growing steadily, not only due to their structural versatility but also for their potential applications in the fields of solid acid electrolytes[1] and materials with nonlinear optical properties.[2] The anionic substructures of conventional borosulfates are similar to silicates and consist of vertex connected (BO_4) and (SO_4) tetrahedra. Accordingly, oligomeric anions like in the potassium borosulfate $K_5[B(SO_4)_4]$,[3] anionic chains[4–11] and layers[12–14] as well as extended 3D networks[4,15] have been discovered in the recent years. In contrast to alumosilicates, where Al–O–Al bonds are unexpected according to Loewenstein's rule,[16] several borosulfates with S–O–S[4,5,7,17,18] and even B–O–B[11,19–22] bridges are known. Hitherto, borosulfates with anionic chains are particularly numerous, whereas 3D networks are scarce. In contrast to the diversity of the anionic substructure, so far the cations are mainly monoatomic or, for example, ammonium[5] and hydronium.[7]

Our latest findings serve not only to extend the list of cations for borosulfates substantially, but prove that borosulfates are able to stabilise also cluster-like aggregates.

Results and Discussion

The reaction of $AuCl_3$ with boric acid and SO_3 at elevated temperatures in evacuated and torch-sealed glass ampoules (details in the experimental section) leads to crystals of $[Au_3Cl_4][B(S_2O_7)_2]$ and $[Au_2Cl_4][B(S_2O_7)_2](SO_3)$ (Figure S1 in the Supporting Information).

Up to now, most borosulfates have been synthesised in solvothermal reactions with and in oleum, which means sulfuric acid with a varying amount of SO_3 (20–65 %).[23] The higher proportion of SO_3 for the herein presented reactions leads to an increase in the number of S–O–S bonds in the anionic substructure in comparison to the conventional borosulfates and thus to $[B(S_2O_7)_2]^-$-anions. These anions have been observed before, even for reactions with oleum. However, the cations presented within the new compounds are unusual and especially the chain-like arrangement in $[Au_2Cl_4][B(S_2O_7)_2](SO_3)$ calls for an investigation of the electronic properties, as such pseudo-one-dimensional chains tend to have extraordinary properties.[24] In contrast to the typical syntheses of borosulfates the absence of a protic acid prevents the release of HCl and is, to the best of our knowledge, decisive for the successful syntheses of both new cation topologies. The terminal S–O bonds of the *bis*-disulfatoborate anions $[B(S_2O_7)_2]^-$ (Figure S2) fall in the narrow range of 1.396(6) to 1.420(6) Å for $[Au_3Cl_4][B(S_2O_7)_2]$ and 1.398(5) to 1.407(4) Å for $[Au_2Cl_4][B(S_2O_7)_2](SO_3)$ (Figure S4), whereas the S–O bonds in the B–O–S bridges are on average 1.53 Å for $[Au_3Cl_4][B(S_2O_7)_2]$ and 1.54 Å for $[Au_2Cl_4][B(S_2O_7)_2](SO_3)$, respectively (Table S3, S4 and S7, S8). The S–O bond lengths of the SO_3 molecule amount to 1.374(8) and 1.390(5) Å. These findings exclude the possibility of protonation.

The arrangement of the cationic subunit of $[Au_3Cl_4][B(S_2O_7)_2]$ (Figure 1) can be best described by two formula units.

In the $[Au_6Cl_8]^{2+}$ cation, the gold atoms form octahedra, in which all but the equatorial edges are capped by chloride ions. This arrangement closely resembles the textbook example $Nb_6Cl_{12}^{2+}$, with the essential difference that for the Nb_6 octahedron *all* edges are capped by the chloride anions.[25]

[a] S. Sutorius, Dr. D. van Gerven, Dr. B. Rasche, Dr. J. Bruns
Institute of Inorganic Chemistry, University of Cologne
Greinstrasse 6, 50939 Cologne (Germany)
E-mail: j.bruns@uni-koeln.de
bertold.rasche@uni-koeln.de
[b] Dr. S. Olthof
Institute of Physical Chemistry, University of Cologne
Greinstrasse 4, 50939 Cologne (Germany)

Supporting information for this article is available on the WWW under https://doi.org/10.1002/chem.202200004

Research Article
doi.org/10.1002/chem.202200004

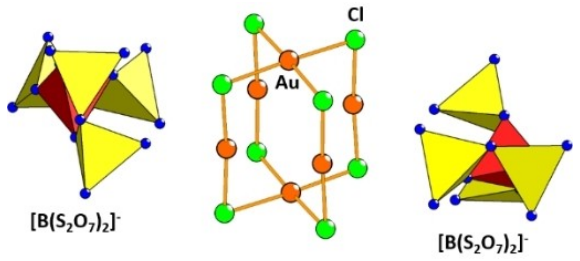

Figure 1. *Bis*-disulfatoborate anions around the $[Au_6Cl_8]^{2+}$ cation in the structure of $[Au_3Cl_4][B(S_2O_7)_2]$.

For $[Au_3Cl_4][B(S_2O_7)_2]$ the Au–Cl distances are in the narrow range of 2.305(2) to 2.321(2) Å. The Au–Au distances are on average 3.23 Å with no significant distortion of a perfect Au_6 octahedron. The equatorial edges are capped by oxygen atoms (Au–O distances >2.8 Å), however the oxygen atoms are not located in plane with the edges, but shifted up- and downwards for the opposite located oxygen atoms, respectively (Figure S3). Furthermore, all gold atoms of the Au_6 octahedron are coordinated to one additional oxygen atom (Au–O distances >3.0 Å). The structure can be best described as a mixed-valent Au^I/Au^{III}-chloride cation according to the formula $[Au^{III}_2Au^I_4Cl_8][B(S_2O_7)_2]_2$, with Au^{III} being in square planar and Au^I in linear coordination of chloride anions. This assumption is in good agreement with the Au–Cl bond lengths of AuCl[26] (on average 2.30 Å) and $AuCl_3$[27] (on average 2.35 Å for the non-terminal positions of the Au_2Cl_6 dimers) and further corroborated by the Mulliken charges from the density-functional theory (DFT) based calculations (Au^{III}: $+0.7$ vs. Au^I: $+0.4$; Table S9). It shall be noted that Mulliken charges do not allow a quantitative estimation of oxidation states, but provide a qualitative argument when comparing the same atom type within the same structure or within similar representatives. The resulting $[Au_6Cl_8]^{2+}$ cations are separated by $[B(S_2O_7)_2]^-$ anions (Figure 2).

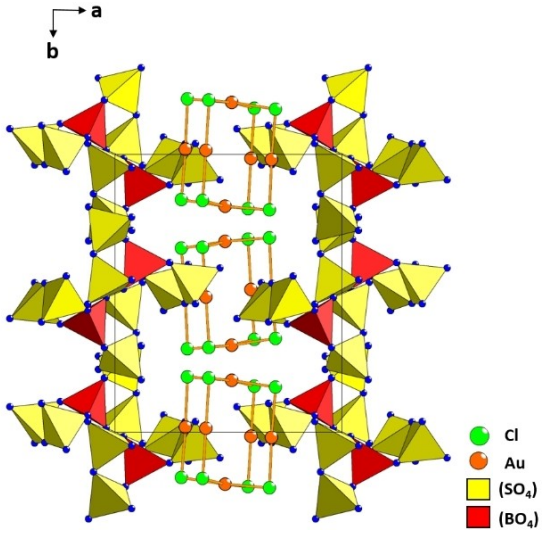

Figure 2. Crystal structure of $[Au_3Cl_4][B(S_2O_7)_2]$ in projection on the *ab*-plane.

The crystal structure of $[Au_2Cl_4][B(S_2O_7)_2](SO_3)$ contains the same disulfatoborate anion $[B(S_2O_7)_2]^-$ as the cluster compound and additionally one molecule SO_3 per $[B(S_2O_7)_2]^-$ anion (Figure S4). The cationic substructure is composed of gold atoms coordinated in a square planar manner by chloride ions according to the Niggli formula ${}_\infty{}^1\{[AuCl_{4/2}AuCl_{4/2}]^+\}$ and runs in a wave-like pattern parallel to the crystallographic *a*-axis (Figure 3). The cations and anions are packed in a layer-like arrangement along the crystallographic *c*-axis (Figure 4). The Au–Cl distances are on average 2.29 and 2.42 Å for the two crystallographically different gold cations, respectively. This finding hints toward the presence of two different oxidation states for the gold cations, namely the typical +III and the uncommon +II. This assumption is further supported by the Mulliken charges from the DFT calculations (Au^{III}: $+0.8$ and Au^{II}: $+0.6$; Table S10), particularly considering the cluster compound

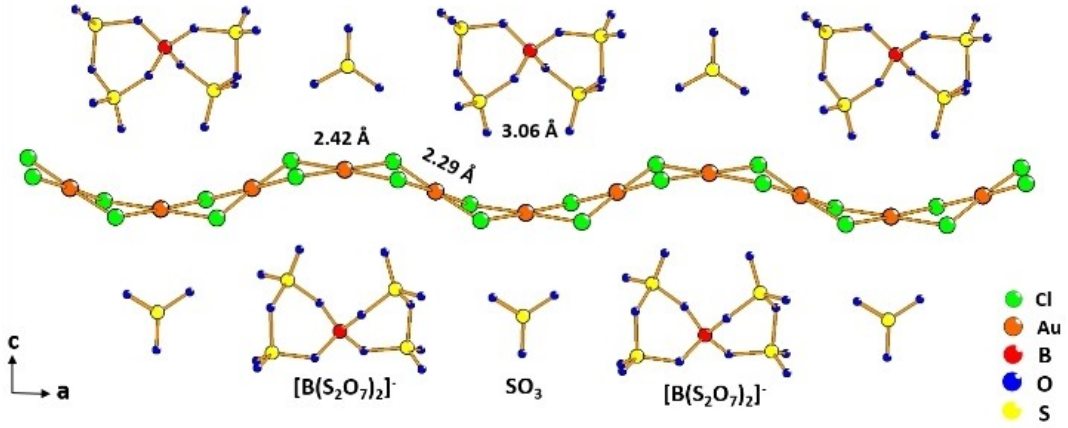

Figure 3. Cationic chains running parallel to the crystallographic *a*-axis in the crystal structure of $[Au_2Cl_4][B(S_2O_7)_2](SO_3)$. The numbers indicate the average Au–Cl bond lengths of the different Au cations and the shortest distances of two terminal oxygen atoms in the $[B(S_2O_7)_2]^-$ anion.

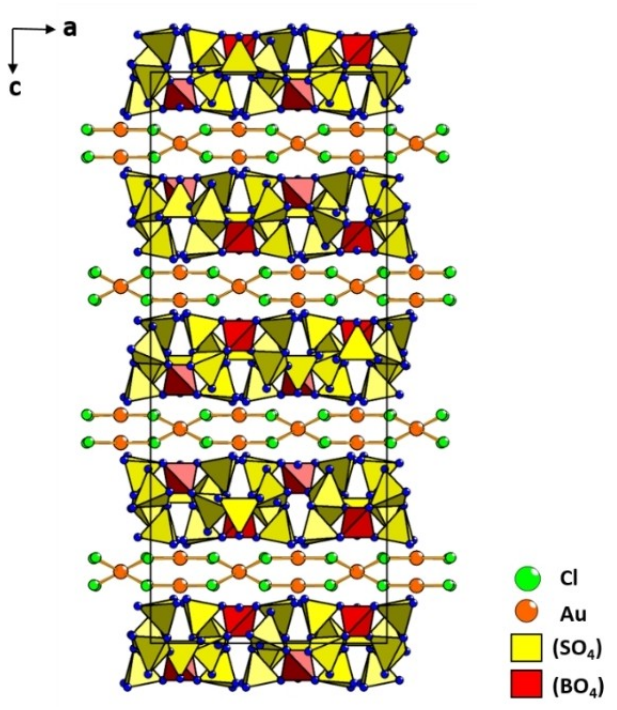

Figure 4. Crystal structure of $[Au_2Cl_4][B(S_2O_7)_2](SO_3)$ in projection onto the crystallographic *ac*-plane.

as reference in which the Au^{III} yields a comparable charge of $+0.7$ while the Au^{I} yields a charge of $+0.4$.

According to the single crystal X-ray data, further impurities can be excluded. The residual electron density is low and the terminal S–O bonds are not elongated, thus protonation can be excluded as well.

Accordingly, we have to assume that the gold atoms with short Au–Cl bonds are trivalent, whereas the gold atoms with longer Au–Cl bonds are divalent. It is noteworthy that the $[B(S_2O_7)_2]^-$ anions are twisted in a manner that the distance between two different terminal oxygen atoms is comparably short (3.06 Å). The Au^{III} cations are additionally coordinated by two $[B(S_2O_7)_2]^-$ anions, respectively. However, the Au^{III}–O distances are >2.8 Å.

In contrast to Au^{I} and Au^{III}, Au^{II} species are comparably rare. Examples are the mixed-valent fluoride $Au[AuF_4]_2$[28] as well as $Au(SO_4)$,[29] with the latter exhibiting Au–Au dumbbells. Furthermore, several gold xenon complexes have been structurally characterised, for example $[AuXe_4][Sb_2F_{11}]_2$, [*trans*-$AuXe_2][SbF_6]_2$, [*cis*-$AuXe_2][Sb_2F_{11}]_2$ and $[(\mu\text{-F})\text{-}Au_2Xe_2][SbF_6]_3$.[30] In the field of metal–organic chemistry, a remarkable example is the neutral (porphyrinato)gold(II) complex with its square planar coordination of the central Au^{II}.[31]

As crystals from both structures could not be grown separately, the characterisation beyond single crystal X-ray diffraction is difficult. In addition, the crystals suffer from the release of SO_3 while grinding in a mortar. Thus, the preparation of a suitable sample for PXRD was so far not successful. Accordingly, we cannot exclude additional phases in the product mixture.

However, XPS measurements on a grounded sample prepared under strict exclusion of O_2 and H_2O showed the expected core level signals (Figure S5) and Au oxidation states (Figure S6) and therefore support our assumption of mono-, di- and trivalent gold cations in the investigated mixture (Figure S6). Because the products contained Au^{I} and Au^{II}, the starting material $AuCl_3$ is reduced at least partially. Besides the formation of Cl_2, which can be identified by the slightly greenish colour of the gas in the ampoule after the reaction, the formation of O_2 and SO_2 from SO_3 cannot be excluded.

The electronic structure of $[Au_3Cl_4][B(S_2O_7)_2]$ yields flat bands (Figure S9) and a substantial band gap of 0.7 eV in the density of states (DOS) at the Fermi level (Figure 5, left). While this means that the compound definitely has a band gap, quantitatively the latter value has to be considered with care as is true for any DFT calculation without additional corrections. This electronic band gap at the Fermi level and the flat bands (Figure S9) match with a structure in which clusters are electronically well separated.

Calculation of the electronic structure for $[Au_2Cl_4][B(S_2O_7)_2](SO_3)$ immediately reveals a fundamentally different behaviour compared to the cluster-like compound. In the DOS one finds relatively localised states close to the Fermi level, with a pseudo gap directly at the Fermi level (Figure 5). The latter resembles the zero-gap behaviour as known from graphene.[32] Employing the projected DOS these states at the Fermi level can be attributed to the gold d orbitals and chlorine p orbitals (Figure S8). Inspecting the electronic structure more closely, an unusual linear dispersion of the bands at the Fermi energy of approximately 0.35 eV along the direction of the gold strands (Figure 6) can be found. In contrast, the same bands are almost perfectly flat in all directions perpendicular to the gold strands (Figure 6). This indicates that the structure has a very strong one-dimensional character and because spin-orbit coupling does not split the bands at the Fermi level, as would be expected for a topological insulator,[33] the gold-chloride strands

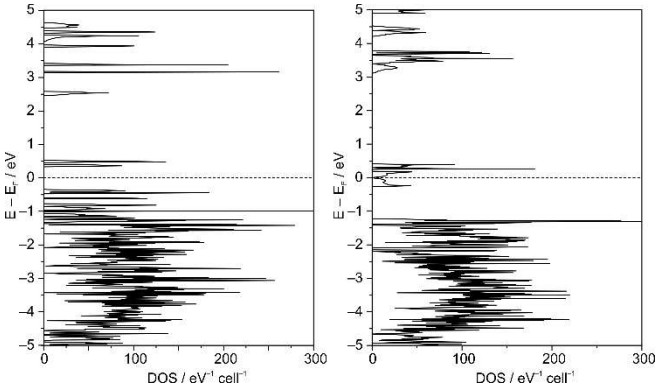

Figure 5. Projected density of states for $[Au_3Cl_4][B(S_2O_7)_2]$ (left) and $[Au_2Cl_4][B(S_2O_7)_2](SO_3)$ (right) from a full-relativistic DFT calculation of the relaxed structures.

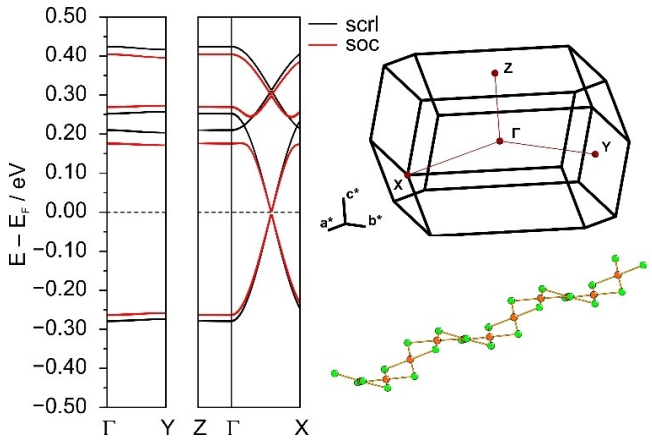

Figure 6. Scalar (black; scrl) and full (red; soc) relativistic electronic band structures of $[Au_2Cl_4][B(S_2O_7)_2](SO_3)$ along selected directions (left) in the first Brillouin zone (right). The orientation of the gold strands in relation to the Brillouin zone is shown at the bottom.

can be considered as well-isolated one-dimensional metallic wires.

Such a situation of a one-dimensional metal is also found for the famous Krogmann salts, with stacks of planar $Pt(CN)_4$ units forming a chain.[34] In the latter case, the strongly anisotropic electronic behaviour can be observed experimentally under a microscope using polarised light. Because electrons are only mobile along and not perpendicular to the strands, absorption can only appear for light polarised within a plane parallel to the metallic chains. This strong direction dependent polarisability means that the absorption and luster expected for a metal is only observed for light polarised in this fashion. Precisely such a behaviour shows the compound $[Au_2Cl_4][B(S_2O_7)_2](SO_3)$. The shape of the crystals allows to orient the gold-strands with respect to the polarised light. In doing so, the crystals show up as black with metallic lustre. Turning the crystals subsequently and therefore arranging the gold strands non-parallel to the polarisation plane reveals the same crystals as transparent and greenish (Figure 7 and Video in the Supporting Information).

Since Krogmann's exploration, several other organic and inorganic one-dimensional metals have been discovered.[35,36] With our experimental findings we complement the theoretical work on the electronic structure of one-dimensional halogen-bridged gold chains.[24e]

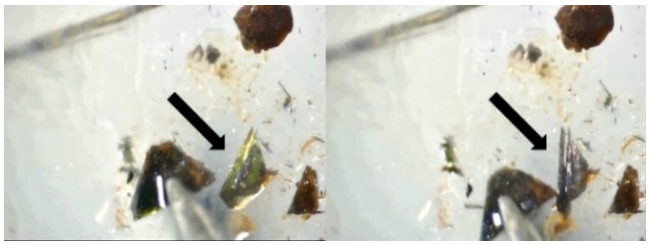

Figure 7. Crystal of $[Au_2Cl_4][B(S_2O_7)_2](SO_3)$ under a polarisation microscope with the polarised light perpendicular (left) and parallel (right) to the cationic strands.

Conclusion

In summary, we have presented the synthesis of two new borosulfates with polycationic substructures, namely $[Au_3Cl_4][B(S_2O_7)_2]$ with a cluster-like arrangement and $[Au_2Cl_4][B(S_2O_7)_2](SO_3)$ with a chain-like arrangement. Both are obtained in the same solvothermal reaction with and in SO_3. XPS measurements complement the finding of mono- and trivalent gold cations for $[Au_3Cl_4][B(S_2O_7)_2]$ as well as di- and trivalent cations for $[Au_2Cl_4][B(S_2O_7)_2](SO_3)$. The electronic structure of $[Au_2Cl_4][B(S_2O_7)_2](SO_3)$ reveals the very unusual one-dimensional character of this compound. Microscopy with polarised light supports these findings and levels the playing field for future transport measurements. Furthermore, the synthetic pathway to borosulfates through reaction with and in SO_3 opens new possibilities to stabilise atypical cations.

Experimental Section

CAUTION! SO_3 is a strong oxidiser, which needs careful handling. During and even after the reaction, the ampoule might be under remarkable pressure. The ampoule must be cooled with liquid nitrogen prior to opening.

Synthesis of $[Au_3Cl_4][B(S_2O_7)_2]$ and $[Au_2Cl_4][B(S_2O_7)_2](SO_3)$: $AuCl_3$ (30 mg (0.1 mmol), synthesised according to ref. [1]) and H_3BO_3 (75 mg (1.21 mmol), Carl Roth, Karlsruhe, Germany, $\geq$99.8 %) were loaded into a thick-walled glass ampoule (l = 200 mm, ø = 16 mm, thickness of the tube wall = 1.8 mm) and attached to a specially designed apparatus for the generation, handling and titration of SO_3 under inert atmosphere. To generate SO_3, Oleum (20 % SO_3, Sigma–Aldrich) was added dropwise to an excessive amount P_4O_{10} (97 %, Merck). Additionally, SO_3 can be transferred to the gaseous phase by heating the P_4O_{10} containing flask with an oil bath to 130 °C. The pressure within the apparatus can be monitored by a Teflon-lined manometer, which is attached above the dropping funnel. SO_3 condenses and accumulates in a burette, which is part of the specially designed apparatus and accessible after opening a Teflon-lined valve. Finally, liquid SO_3 can be titrated into the underneath the burette attached ampoule. For the synthesis of the title compounds is an amount of 0.4 mL SO_3 needed. Additionally, the ampoule will be torch sealed under reduced pressure and placed in a box-shaped furnace. The ampoule was heated to 363 K within 24 h. The temperature was maintained for 48 h and finally reduced to 298 K with a cooling rate of 0.01 K min^{-1}. Following the initial reaction, the mother liquor was separated from the crystals by decantation.

Structural analysis

X-ray crystallography: The following has been conducted at the electron synchrotron DESY in Hamburg.

The SO_3-containing side of the ampoule was cooled with liquid nitrogen and several crystals were transferred into inert oil, directly after opening. Yellow needles of $[Au_3Cl_4][B(S_2O_7)_2]$ and black blocks of $[Au_2Cl_4][B(S_2O_7)_2](SO_3)$ were isolated and prepared for the single crystal X-ray measurements (Figure S1). Therefore, several crystals

were transferred into inert perfluorpolyalkyl ether oil (ABCR chemicals, Karlsruhe, Germany) directly after opening of the ampoule. Under a polarisation microscope, crystals were prepared, mounted onto a loop (MicroMounts, MiTeGen LLC, New York, USA) and immediately placed into a stream of cold N_2 (100.0(1) K) inside the diffractometer. After unit cell determination, the reflection intensities were collected.

$[Au_3Cl_4][B(S_2O_7)_2]$: yellow needles (0.28×0.175×0.17 mm), monoclinic, $P2_1/c$, $Z=4$, $a=10.6266(3)$ Å, $b=12.7938(4)$ Å, $c=12.7373(4)$ Å, $\beta=99.322(3)°$, $V=1708.82(9)$ Å^3, $\rho=4.259$ g cm^{-3}, $2\theta_{max.}=35.0°$, $\lambda(Mo_{K\alpha})=50.014$ pm, 24116 reflections, 3111 unique reflections ($R_{int}=0.0704$), empirical absorption correction using spherical harmonics, implemented in SCALE3 ABSPACK scaling algorithm and an additional spherical absorption correction (program CrysAlisPro 1.171.41.121a (Rigaku OD, 2021)), structure solution by dual methods using ShelXT,[2] full-matrix-least-squares refinement (235 parameters) against $|F^2|$ by ShelXL,[3] anisotropic displacement parameters for all atoms (program CrysAlisPro 1.171.41.121a (Rigaku OD, 2021)), $R_1=0.0277$, $wR_2=0.0617$ for all reflections with $I>2\sigma(I_0)$ and $R_1=0.345$, $wR_2=0.0641$ for all 24116 reflections, max./min. residual electron density = 1.51/−1.25 e$^-$ Å^{-3}.

$[Au_2Cl_4][B(S_2O_7)_2](SO_3)$: black blocks of metallic lustre (0.2×0.15×0.1 mm), orthorhombic, *Fddd*, $Z=16$, $a=13.1467(4)$ Å, $b=17.8576(6)$ Å, $c=31.711(1)$ Å, $V=7444.8(4)$ Å^3, $\rho=3.49$ g cm^{-3}, $2\theta_{max.}=38.0°$, $\lambda(Mo_{K\alpha})=50.014$ pm, 22883 reflections, 2161 unique reflections ($R_{int}=0.0656$), empirical absorption correction using spherical harmonics, implemented in SCALE3 ABSPACK scaling algorithm and an additional spherical absorption correction (program CrystAlisPro 1.171.40–84a: Rigaku Pxford Diffraction, 2020), structure solution by dual methods using ShelXT,[2] full-matrix-least-squares refinement (134 parameters) against $|F^2|$ by ShelXL,[3] anisotropic displacement parameters for all atoms (program CrysAlisPro 1.171.41.121a (Rigaku OD, 2021)), $R_1=0.0248$, $wR_2=0.0495$ for all reflections with $I>2\sigma(I_0)$ and $R_1=0.0378$, $wR_2=0.0533$ for all 22883 reflections, max./min. residual electron density = 1.20/−1.09 e$^-$ Å^{-3}.

Further details are listed in Table S1 and S5. Deposition Numbers 2069076 for $[Au_3Cl_4][B(S_2O_7)_2]$ and 2069073 and $[Au_2Cl_4][B(S_2O_7)_2](SO_3)$ contains the supplementary crystallographic data for this paper. These data are provided free of charge by the joint Cambridge Crystallographic Data Centre and Fachinformationszentrum Karlsruhe Access Structures service.

X-ray photoelectron spectroscopy: X-ray photoelectron spectroscopy (XPS) measurements were conducted using a non-monochromated $Mg_{K\alpha}$ excitation at 1253.6 eV. The material was finely grounded under N_2 atmosphere and applied with a brush as a thin layer onto a conductive adhesive tape. The material was transferred into the vacuum system without air exposure. For the XPS survey scan a pass energy of 100 eV was chosen, while for the detailed scan this was reduced to 10 eV to achieve better energy resolution. Peak fitting was done using the software "XPS Peak Fit" employing a Shirely background and Voigt profiles.

Quantum chemical methodology: All scalar- and full-relativistic calculations were performed with the full-potential local-orbital (FPLO) code version 18.00,[4] within the local density approximation (LDA) using the parametrisation PW92.[5] The Blöchl corrected linear tetrahedron method was employed for $[Au_3Cl_4][B(S_2O_7)_2]$ with a 6×6×6 k-mesh and for $[Au_2Cl_4][B(S_2O_7)_2](SO_3)$ with a 8×8×8 k-mesh (approximately 80 k-points Å), after checking for convergence with respect to the number of k-points. Spin–orbit coupling (SOC) was implemented on the level of the four-component Dirac equation. The basis states that were treated as valence states are listed in Table S9.

Acknowledgements

We acknowledge DESY (Hamburg, Germany), a member of the Helmholtz Association HGF, for the provision of experimental facilities. Parts of this research were carried out at PETRA 3, and we would like to thank Dr. Carsten Paulmann for assistance in using the provided equipment. Beamtime was allocated for proposal I-20191280. J.B. thanks the Fonds der Chemsichen Industrie (FCI) for financial support. B.R. thanks the FCI for funding through a Liebig group. The authors thank Prof. Michael Ruck (TU Dresden) for the helpful discussion at the HäKo 2021 in Bayreuth and Prof. Mathias Wickleder for constant support. Open Access funding enabled and organized by Projekt DEAL.

Conflict of Interest

The authors declare no conflict of interest.

Data Availability Statement

The data that support the findings of this study are available in the supplementary material of this article.

Keywords: borosulfates · crystal structures · electronic structures · one-dimensional metals · polycations

[1] M. D. Ward, B. L. Chaloux, M. D. Johannes, A. Epshteyn, *Adv. Mater.* **2020**, *32*, 2003667.
[2] L. Kang, X. Liu, Z. Lin, B. Huang, *Phys. Rev. B* **2020**, *102*, 205424.
[3] H. A. Höppe, K. Kazmierczak, M. Daub, K. Förg, F. Fuchs, H. Hillebrecht, *Angew. Chem. Int. Ed.* **2012**, *51*, 6255–6257; *Angew. Chem.* **2012**, *124*, 6359–6362.
[4] M. Daub, K. Kazmierczak, P. Gross, H. Höppe, H. Hillebrecht, *Inorg. Chem.* **2013**, *52*, 6011–6020.
[5] M. Daub, H. A. Höppe, H. Hillebrecht, *Z. Anorg. Allg. Chem.* **2014**, *640*, 2914–2921.
[6] J. Bruns, M. Podewitz, O. Janka, R. Pöttgen, K. Liedl, H. Huppertz, *Angew. Chem. Int. Ed.* **2018**, *130*, 9548–9552.
[7] M. Daub, K. Kazmierczak, H. A. Höppe, H. Hillebrecht, *Chem. Eur. J.* **2013**, *19*, 16954–16962.
[8] J. Bruns, M. Podewitz, M. Schauperl, K. Liedl, O. Janka, R. Pöttgen, H. Huppertz, *Eur. J. Inorg. Chem.* **2017**, 3981–3989.
[9] S. Schönegger, J. Bruns, B. Gartner, K. Wurst, H. Huppertz, *Z. Anorg. Allg. Chem.* **2018**, *644*, 1702–1706.
[10] P. Netzsch, H. A. Höppe, *Z. Anorg. Allg. Chem.* **2020**, *646*, 1563–1569.
[11] P. Netzsch, P. Gross, H. Takahashi, H. A. Höppe, *Inorg. Chem.* **2018**, *57*, 8530–8539.
[12] J. Bruns, M. Podewitz, M. Schauperl, B. Joachim, K. Liedl, H. Huppertz, *Chem. Eur. J.* **2017**, *23*, 16773–16781.
[13] L. C. Pasqualini, O. Janka, S. Olthof, H. Huppertz, K. Liedl, M. Podewitz, J. Bruns, *Chem. Eur. J.* **2020**, *26*, 17405–17415.
[14] P. Netzsch, F. Pielnhofer, R. Glaum, H. A. Höppe, *Chem. Eur. J.* **2020**, *26*, 14745–14745.
[15] M. Hämmer, L. Bayarjargal, H. A. Höppe, *Angew. Chem. Int. Ed.* **2021**, *60*, 1503–1506; *Angew. Chem.* **2021**, *133*, 1525–1529.
[16] W. Loewenstein, *Am. Mineral.* **1954**, *39*, 92–96.
[17] P. Netzsch, H. A. Höppe, *Inorg. Chem.* **2020**, *59*, 18102–18108.
[18] P. Netzsch, H. A. Höppe, *Eur. J. Inorg. Chem.* **2020**, 1065–1070.
[19] P. Gross, A. Kirchhain, H. A. Höppe, *Angew. Chem. Int. Ed.* **2016**, *55*, 4353–4355; *Angew. Chem.* **2016**, *128*, 4426–4428.
[20] C. Logemann, M. S. Wickleder, *Angew. Chem. Int. Ed.* **2013**, *52*, 14229–14232; *Angew. Chem.* **2013**, .

[21] M. Daub, H. Hillebrecht, *Eur. J. Inorg. Chem.* **2015**, 4176–4181.
[22] P. Netzsch, P. Gross, H. Takahashi, S. Lotfi, J. Brgoch, H. A. Höppe, *Eur. J. Inorg. Chem.* **2019**, 3975–3981.
[23] J. Bruns, H. A. Höppe, M. Daub, H. Hillebrecht, H. Huppertz, *Chem. Eur. J.* **2020**, *26*, 7966–7980.
[24] a) J. M. Luttinger, *J. Math. Phys.* **1963**, *4*, 1154–1162; b) H. Wagner, H. P. Geserich, R. v. Baltz, K. Krogmann, *Solid State Commun.* **1973**, *13*, 659–663; c) T. Giamarchi, *Chem. Rev.* **2004**, *104*, 5037–5056; d) B. Rasche, M. Ruck, *Inorg. Chem.* **2018**, *57*, 5507–5513; e) C. Janiak, R. Hoffmann, *Inorg. Chem.* **1989**, *28*, 2743–2747; f) L. V. Interrante, F. P. Bundy, *J. Inorg. Nucl. Chem.* **1977**, *39*, 1333–1337.
[25] U. Müller, *Anorganische Strukturchemie*, Vieweg + Teubner, 6. Ed., **2008**.
[26] J. Strähle, K. P. Lörcher, *Z. Naturforsch.* **1974**, *B29*, 266–267.
[27] P. Schwerdtfeger, P. D. W. Boyd, S. Brienne, A. K. Burrell, *Inorg. Chem.* **1992**, *31*, 3411–3422.
[28] R. Schmidt, B. G. Müller, *Z. Anorg. Allg. Chem.* **1999**, *625*, 605–608.
[29] M. S. Wickleder, *Z. Anorg. Allg. Chem.* **2001**, *677*, 2112–2114.
[30] a) T. Drews, S. Seidel, K. Seppelt, *Angew. Chem. Int. Ed.* **2002**, *41*, 454–456; *Angew. Chem.* **2002**, *114*, 470–473; b) S. Seidel, K. Seppelt, *Science* **2000**, *290*, 117–118; c) K. Seppelt, *Z. Anorg. Allg. Chem.* **2003**, *629*, 2427–2430.
[31] S. Preiß, C. Förster, S. Otto, M. Bauer, P. Müller, D. Hinderberger, H. Haeri, L. Carella, K. Heinze, *Nat. Chem.* **2017**, *9*, 1249–1255.
[32] B. Rasche, A. Isaeva, M. Ruck, S. Borisenko, V. Zabolotnyy, B. Büchner, K. Koepernik, C. Ortix, M. Richter, J. van den Brink, *Nat. Mater.* **2013**, *12*, 422–425.
[33] B. Rasche, A. Isaeva, M. Ruck, S. Borisenko, V. Zabolotnyy, B. Büchner, K. Koepernik, C. Ortix, M. Richter, J. van den Brink, *Nat. Mater.* **2013**, *12*, 422–425.
[34] K. Krogmann, *Angew. Chem. Int. Ed.* **1969**, *8*, 35–42.
[35] B. Wahl, L. Kloo, M. Ruck, *Z. Anorg. Allg. Chem.* **2009**, *635*, 1979–1985.
[36] a) A. Troisi, *Nat. Mater.* **2009**, *8*, 538–539; b) Y. Yoshida, H. Kitagawa, *Chem. Commun.* **2020**, *56*, 10100–10112.

Manuscript received: January 2, 2022
Accepted manuscript online: March 8, 2022
Version of record online: March 23, 2022